An Efficient Capacitor Voltage Balancing Scheme for Modular Multilevel Converter Based Wind Energy Conversion System

Ahmet Mete VURAL[1], Mehmet KURTOĞLU[1,2], Fatih EROĞLU[1]
[1]*Electrical-Electronics Engineering Department, Gaziantep University, Gaziantep, Turkey*
[2]*Electrical-Electronics Engineering Department, Iskenderun Technical University, Hatay, Turkey*
mkurtoglu@gantep.edu.tr

***Abstract*—Modular multilevel converters (MMCs) can be a reliable solution since they have modular structure and high quality output waveform for permanent magnet synchronous generator (PMSG) based wind energy conversion system (WECS). Capacitor voltage balancing in nearest level modulation (NLM) is required to keep the capacitor voltage of each submodule of MMC constant. In this paper, an efficient capacitor voltage balancing scheme under NLM is proposed for PMSG based WECS with MMC topology. Through proposed control scheme, arm voltages are separately controlled and voltage ripple of around 1.5% is obtained. This result provides high quality output waveform at the point of common coupling (PCC). Furthermore, DC-link voltage control is achieved via hysteresis current control based proportional-integral controller. The ripple of DC-link voltage is obtained quite well as nearly 0.25%. In addition, load voltage control is accomplished using dq reference frame-based voltage control scheme for voltage and frequency stabilization at the PCC by regulating the voltage at its reference value. Simulation studies show that all proposed control schemes give satisfactory results for MMC based WECS under variable dynamic operation modes. Finally, experimental verification is performed using laboratory prototype to show the applicability of the proposed capacitor voltage balancing scheme.**

***Index Terms*—converters, permanent magnet machines, power conversion, power system modeling, wind energy integration.**

I. INTRODUCTION

Renewable energy sources are becoming more common and utilization of them is increasing in recent years. Wind energy is one of the considerable renewable energy sources, which is attractive in terms of cleanness and sustainability. In recent years, wind energy is used to supply power to both grid and stand-alone loads [1-5]. Generated energy from the wind turbine system must be transmitted into the grid or load by ensuring some conditions such as desired voltage and frequency. For this purpose, a generator is necessary to convert the wind energy from mechanical to electricity form. Permanent magnet synchronous generator (PMSG) is frequently preferred in wind energy applications since it enables self-excitation ability, high efficiency, direct-drive and variable speed operation [6-9]. Variable AC energy from the PMSG is transferred to the grid or load with the help of a power electronic interface. This interface is usually constructed from back-to-back converters with a common DC-link. PMSG with a wind turbine and a power electronic interface is called as wind energy conversion system (WECS) [10]. There are several converter topologies that have been adopted for WECS. One of the most prominent converter types is the voltage source converter (VSC) which is operated by a DC voltage formed by a capacitor. Traditional two-level VSC needs big size and high-cost harmonic filter to reduce the output harmonics. However, multilevel converters (MCs) have good output waveform and reduced filter size when compared to two-level VSC [11-12]. Modular multilevel converter (MMC) is an attractive version of the MCs, which has superior features such as modularity, output harmonic performance, high reliability and efficiency [13]. In this regard, an MMC topology can be used as the power electronic interface in WECS. The other benefits of MMC to be used in WECS are the modular submodule (SM) configuration in the power circuit as well as decreased harmonic content owing to the increased voltage level at the output.

In the existing literature, publications related to the WECS based on different power converter types are presented as follows. A new inverter scheme is proposed in [14] for low power WECS. The implemented system includes a battery charge unit as well as PMSG and inverter, and tested by giving improved current total harmonic distortion (THD) results under various rotor speed conditions. Research presented in [15] develops a matrix converter based variable speed WECS. The proposed WECS is validated by both simulation and experimental work by providing satisfactory input and output waveforms. The goal of [16] is to present the application of modular multilevel matrix converter based WECS. In the suggested WECS, the entire control system models are addressed in detail and adequate system performance is obtained in simulation and experimental work with capacitor voltage balancing in the clusters under fixed and variable speed operation. Contribution of [17] is to present a novel hybrid MMC topology for PMSG based WECS. In the grid side, serially connected full-bridge SMs with MMC are structured while neutral-point-clamped converter is added in the generator side. With the developed configuration, higher DC voltage utilization is achieved. The suitability of the overall control scheme is proven by simulations. The purpose of [18] is to suggest the dynamic control of the active and reactive power for diode-clamped multilevel inverter based WECS in grid connected mode. The proposed control system allows controlling the active and reactive power separately with

Digital Object Identifier 10.4316/AECE.2021.04004

harmonic minimization. Capacitor voltage balancing of a diode-clamped inverter is carried out through external circuits. Applicability of the developed control scheme is shown under various dynamic conditions using simulation studies. In [19], a control method including speed and DC-bus voltage control using proportional-integral (PI) regulator is developed for PMSG based WECS. The feasibility of the presented control approach is represented via simulations. The primary concept of [20] is to introduce a new algorithm to control DC-link voltage at the reference point for standalone PMSG based WECS. With the aid of DC-link voltage control, AC output voltage of the load side inverter at the point of common coupling (PCC) is kept fixed regardless of the rotor speed and load changes. Overall control methodology is developed using phase-shifted pulse width modulation (PWM) technique for back-to-back connected MMC based WECS in [21]. In order to accomplish the difficulties in WECS, a circulating current injection method and low voltage ride through ability are presented. Power loss and reliability analysis of a hybrid MMC including half-bridge and full-bridge SMs is discussed by [22] for offshore wind turbines. In the meantime, MMC based PWM rectifier system is presented to increase the equivalent switching frequency by keeping unaffectedly the real switching frequency for PMSG based WECS in [23]. The authors of [24] introduce a minimal capacitor ripple control technique in MMC based WECS. The capacitor voltage ripple of MMC SMs is decreased using the proposed technique irrespective of the maximum power point tracking of WECS. Acceptability of the presented method is validated by simulation study. The intention of [25] is to exhibit an optimization method by considering cost and reliability targets for a hybrid MMC based offshore DC wind turbine. The reliability is provided under steady-state and DC faulted scenarios thanks to the DC fault blocking of hybrid MMC topology. The main target of [26] is to present the three-level boost and MMC based WECS, which incorporates PMSG and passive rectifier. DC-link and MMC capacitor voltage control are provided through the proposed control strategy in grid connected mode.

Research presented in [27] develops a steady-state analysis for MMC based WECS. In the proposed system, MMC that is directly connected to the PMSG is used as a rectifier to convert the AC power obtained from PMSG into DC power. The suitability of the developed steady-state method is confirmed by both simulation and experimental results.

As it can be understood from all studies mentioned above, the usage of MMC in WECS is important in terms of reliable operation thanks to the opportunities of MMC and the studies in this area are few. Although there are similar system topologies in the literature to the designed one in this study, to the best of our knowledge, no study in MMC based WECS focuses in detail on the control of capacitor voltages on SMs of MMC under nearest level modulation (NLM). In this respect, a WECS is suggested in this paper which includes a wind turbine, PMSG, uncontrolled diode rectifier, DC-DC boost converter, MMC and load group. Accordingly, an entire control structure is proposed for the developed WECS. The proposed control structure incorporates DC-DC converter control for DC-link voltage management, capacitor voltage balancing control on MMC SMs and load voltage control. Although DC-link voltage control and load voltage control scheme are available in the literature [28-29], these control models are designed using hysteresis current control with PI controllers and incorporated into the MMC based WECS. The contributions of this work are as follows.

1. MMC, which is one of the attractive converter topology in recent years, is incorporated in the WECS for reliable operation.
2. An efficient SM capacitor voltage balancing scheme under NLM is proposed for a PMSG based WECS having MMC topology.
3. A DC-link voltage regulation method is achieved using hysteresis current control-based PI controller under variable dynamic operation modes.
4. The voltage and frequency stabilization at the PCC is accomplished by a voltage control method which is based on dq synchronous reference frame.

This paper is structured as follows. Section II explains the MMC circuit topology. MMC based WECS and overall control concept containing DC-link control, SM capacitor voltage balancing scheme under NLM and load voltage control are given in Section III. Section IV and V provides the simulation and experimental results, respectively. Finally, the conclusion is drawn in Section VI.

II. MMC TOPOLOGY

A general circuit topology of the three-phase MMC is shown in Fig. 1. This topology has a DC side which is supplied from a DC voltage source. When MMC is used in renewable energy applications, the DC power is obtained from the renewable source. MMC contains three phases (legs) and two arms per phase called as upper and lower arm. N series-connected same SMs as well as a series inductor are established in each arm as given in Fig. 1. Voltage level of the MMC is defined depending on the number of SMs in the arm.

Each SM consists of a DC capacitor and two power devices with anti-parallel diodes. This SM cell is called as half-bridge SM (HBSM), given in Fig. 2. These cells are connected in series in both upper and lower arm. HBSM is often preferred due to its easy control ability in MMC based applications [30-31]. Hence, HBSM is adopted in this work. In HBSM, two possible outputs exist as V_C or 0 which are listed in Table 1.

The current i_{arm} represents the arm current. Semiconductor switches S_1 and S_2 operates in opposite manner. Accordingly, if switch S_1 is conducting, SM becomes ON and produces V_C at the output. Contrarily, if switch S_2 is conducting, SM becomes OFF and produces 0 at the output. In this regard, arm voltage is controlled by considering $N_{ON,ij}$, where it states the number of active SMs in an arm. In case of all capacitor voltages on SMs of MMC are balanced and equal to V_C, actual arm voltage is calculated using the equation given as

$$v_{ij} = N_{ON,ij} \times V_C \quad (i = p,n;\ j = a,b,c) \tag{1}$$

where, *pj* and *nj* symbolize the upper and lower arm in phase *j*, respectively.

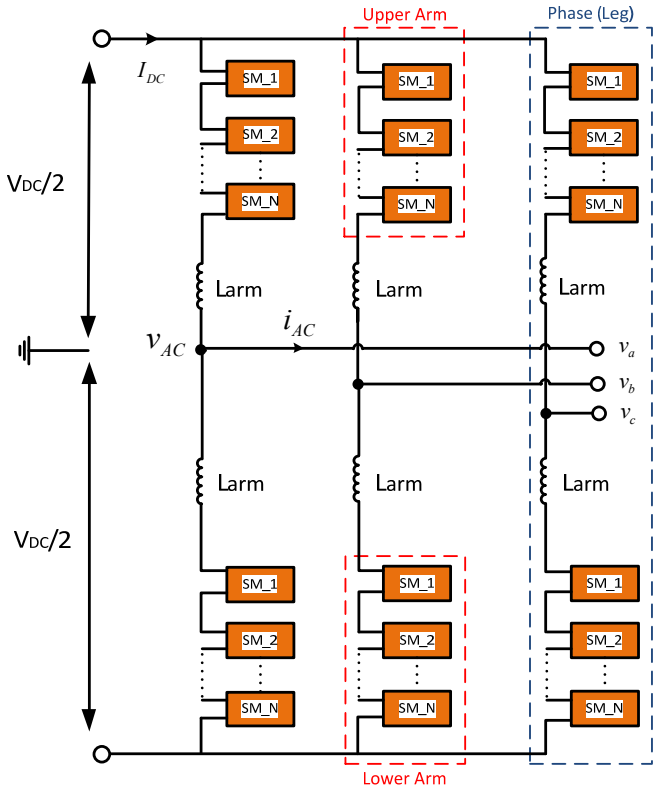

Figure 1. General circuit structure of the three-phase MMC topology

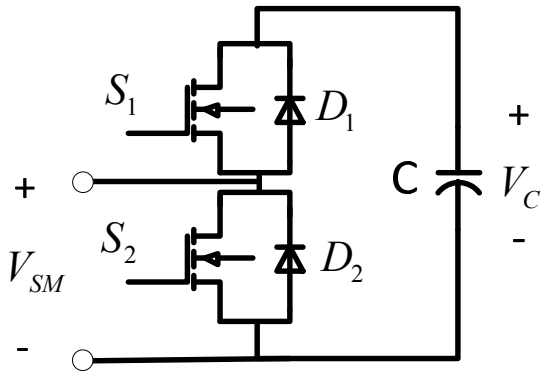

Figure 2. HBSM structure

TABLE I. SWITCHING STATES OF HBSM

S_1	S_2	i_{arm}	Capacitor	V_{SM}
1	0	>0	Charging	V_C
1	0	<0	Discharging	V_C
0	1	>0	Unchanged	0
0	1	<0	Unchanged	0

The equivalent circuit representation of single-phase MMC is illustrated in Fig. 3. Mathematical analysis of MMC is presented for phase-a in the following relations. Arm voltages can be formulated as:

$$V_{a,upper} = \frac{V_{DC}}{2} - V_{a,AC} - L_{arm}\frac{di_{a,upper}}{dt} \quad (2a)$$

$$V_{a,lower} = \frac{V_{DC}}{2} + V_{a,AC} - L_{arm}\frac{di_{a,lower}}{dt} \quad (2b)$$

where, L_{arm} is the arm inductance. Arm equations are given as follows under steady-state condition:

$$V_{a,upper} = \frac{V_{DC}}{2} - V_{a,AC} - v_{a,x} \quad (3a)$$

$$V_{a,lower} = \frac{V_{DC}}{2} + V_{a,AC} - v_{a,x} \quad (3b)$$

where, $v_{a,x}$ denotes the voltage drop on arm inductor. The modulation signal for phase-a can be formulated by:

$$V_{a,AC} = m_i \frac{V_{DC}}{2}\sin(\omega_0 t + \Phi_a) \quad (4)$$

where, m_i, ω_0 and Φ_a are the modulation index, fundamental angular frequency and phase angle, respectively.

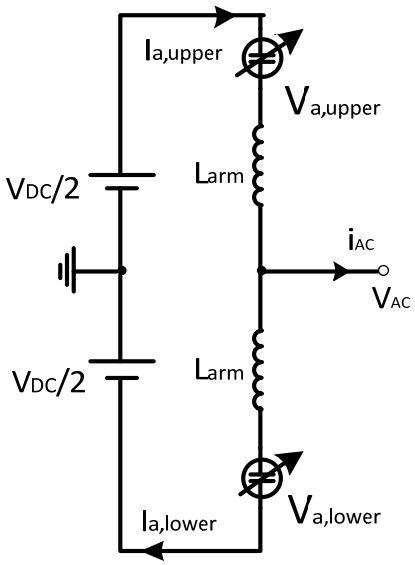

Figure 3. Single phase equivalent circuit of the MMC topology

Arm voltages are deduced for upper and lower arm using Equation (3a), (3b) and (4) as

$$V_{a,upper} = \frac{V_{DC}}{2} - m_i\frac{V_{DC}}{2}\sin(\omega_0 t + \Phi_a) \quad (5a)$$

$$V_{a,lower} = \frac{V_{DC}}{2} + m_i\frac{V_{DC}}{2}\sin(\omega_0 t + \Phi_a) \quad (5b)$$

DC supply voltage can be defined according to the design principle of MMC as

$$V_{DC} = NV_C \quad (6)$$

Replacing (6) into (5a) and (5b) gives

$$V_{a,upper} = \frac{NV_C}{2} - m_i\frac{NV_C}{2}\sin(\omega_0 t + \Phi_a) \quad (7a)$$

$$V_{a,lower} = \frac{NV_C}{2} + m_i\frac{NV_C}{2}\sin(\omega_0 t + \Phi_a) \quad (7b)$$

where, V_C corresponds to the step value of output voltage. If the Equations (7a) and (7b) are normalized, general expressions are obtained for upper and lower arm voltage given as

$$V^{n}_{a,upper} = \frac{N}{2}\left[1 - m_i\sin(\omega_0 t + \Phi_a)\right] \quad (8a)$$

$$V^{n}_{a,lower} = \frac{N}{2}\left[1 + m_i\sin(\omega_0 t + \Phi_a)\right] \quad (8b)$$

III. MMC BASED WECS AND OVERALL CONTROL SCHEME

A. Description of the MMC based WECS

Fig. 4 shows the schematic view of the MMC based WECS topology. It consists of a wind turbine and PMSG which are incorporated as a power generation unit in this study, followed by the diode rectifier, DC-DC boost converter, MMC and the load unit. The fundamental components of the system are described as follows except for MMC. Prime mover of the PMSG is a wind turbine. Since no additional DC source is required in the excitation circuit of PMSG, it is an attractive choice in wind energy applications.

Mathematical model equations of PMSG are stated in dq rotor reference frame in [32] as:

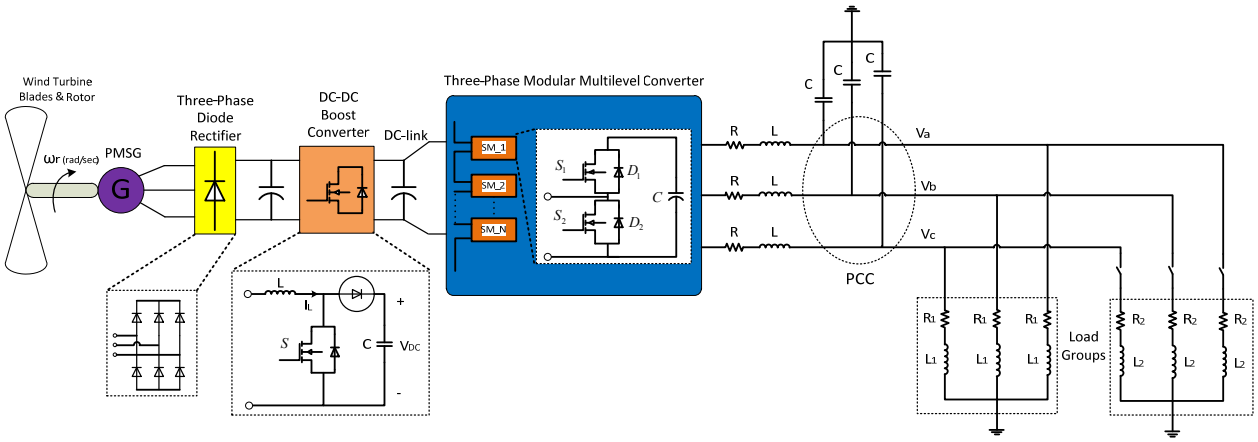

Figure 4. The designed MMC based WECS topology

$$V_d = L_d \frac{di_d}{dt} + R_s i_d - \omega L_q i_q \tag{9}$$

$$V_q = L_q \frac{di_q}{dt} + R_s i_q + \omega L_d i_d + \omega \lambda_m \tag{10}$$

$$T_g = (L_d - L_q) i_q i_d + \lambda_m i_q \tag{11}$$

where, V_d, V_q, i_d, i_q, L_d and L_q denote the stator voltage, current and machine inductance components in dq reference frame while ω, λ_m, T_g and R_s are the electrical frequency, flux linkage, electromagnetic torque and stator resistance, respectively. Three-phase diode rectifier is a simple and inexpensive power conversion device. However, the main disadvantage is that there is no capability to control the power in bidirectional manner. Variable DC voltage is obtained in the output of this rectifier. DC-DC boost converter is also named as step-up converter, whose output voltage is larger than input voltage [33]. Boost converter includes an inductor, a power electronic switch such as MOSFET or IGBT, a diode and a capacitor. The output voltage of the converter is controlled by varying the duty cycle of the power switch used in the converter. Output voltage of the converter is computed with a formula given as

$$V_o = \frac{V_i}{1 - D} \tag{12}$$

where, V_0, V_i and D are the output voltage, input voltage and duty cycle, respectively. Shortly, general introduction of the designed MMC based WECS topology is as follows. The output voltage and frequency of PMSG could increase/decrease with respect to rotor speed under variable speed conditions. Then, the output voltage is converted to DC energy from AC energy via rectifier. For reliable operation, this variable voltage should be controlled and boosted to a fixed value using DC-DC converter, which is regulated with a closed loop feedback control and implemented via PI based hysteresis current control scheme. After that, the controlled DC-link is connected to the MMC which is modulated and controlled using NLM method to obtain constant voltage and frequency at the load side by achieving capacitor voltage balancing in MMC SMs. Therefore, a capacitor voltage balancing scheme under NLM method is developed to control SM voltages. The developed control scheme is implemented separately to the arms of the MMC. Arm voltages are controlled thanks to the proposed control scheme. Moreover, the load voltage control is performed using dq synchronous rotating reference frame-based voltage control scheme for voltage and frequency stabilization at the PCC by regulating the voltage at the reference value.

B. *Control Structures*

DC-link voltage is controlled using DC-DC boost converter circuit. Variable voltage obtained from PMSG at the rectifier output is boosted to a fixed value. The selected reference value for DC-link voltage is regulated through a closed loop feedback control and implemented via hysteresis current control based PI controller. In hysteresis control scheme, the measured inductor current is compared with the produced reference current. Error is limited within a hysteresis band and controller generates the switching sequences for the power switch of the converter [34]. The designed control loop is demonstrated in Fig. 5. After measurement of DC-link voltage, reference inductor current of boost converter is obtained using PI controller. Then, the hysteresis current regulator generates the control pulse for the boost converter. Following the measurement of DC-link voltage, error voltage using reference value is obtained as:

$$V_{DC,error} = V_{DC,ref} - V_{DC,actual} \tag{13}$$

PI regulator produces the reference inductor current that is given below

$$I_{L,ref} = K_p (V_{DC,error}) + K_i \int (V_{DC,error}) dt \tag{14}$$

Error current of the inductor is computed by determining the actual value of it as shown below:

$$I_{error} = I_{L,ref} - I_{L,actual} \tag{15}$$

The switching patterns of the hysteresis control are expressed according to the Equation given below:

$$if\ I_{error} > h;\ \text{then, Switch is ON} \tag{16a}$$

$$if\ I_{error} < h;\ \text{then, Switch is OFF} \tag{16b}$$

where, h indicates the hysteresis band of the controller.

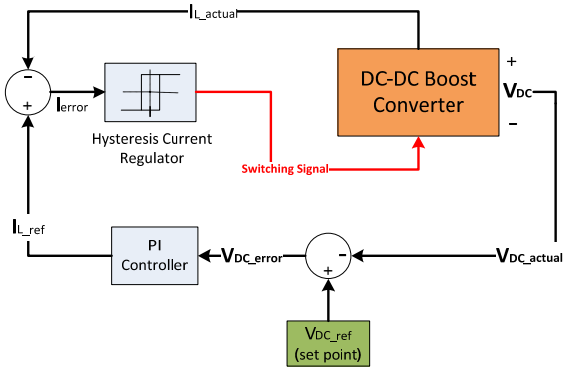

Figure 5. The designed DC-link voltage control scheme

NLM is also called as a staircase modulation, which controls the output voltage simply. When the number of SMs in the arms of MMC is more, THD performance of the output voltage and current is more satisfactory. Fig. 6 depicts the fundamental principle of NLM [35-36]. In this method, each arm of MMC can be controlled separately. The general control diagram of NLM is depicted in Fig. 7.

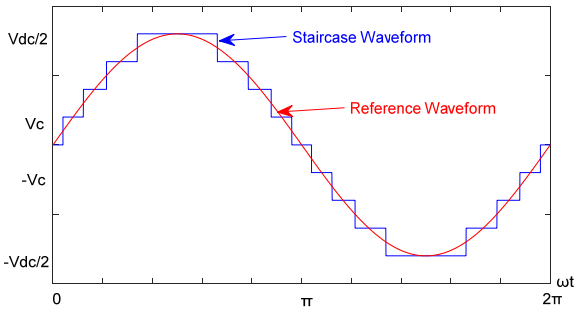

Figure 6. Fundamental principle of NLM

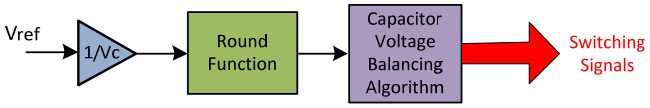

Figure 7. Control implementation of NLM

Instantaneous voltage of upper and lower arm is obtained based on the round function at each sampling frequency. These voltages are given as:

$$m_{a,upper}^{n} = round(V_{a,upper}^{n}) \quad (17a)$$

$$m_{a,lower}^{n} = round(V_{a,lower}^{n}) \quad (17b)$$

where, $m_{a,upper}^{n}$ and $m_{a,lower}^{n}$ denote the instantaneous voltages of arms, respectively. Round function is mathematically formulated as:

$$round(x) = \begin{cases} floor(x); & x < floor(x) + 0.5 \\ ceil(x); & x \geq floor(x) + 0.5 \end{cases} \quad (18)$$

where, *floor(x)* represents the largest integer less than x while *ceil(x)* corresponds to the smallest integer greater than x.

Capacitor voltage balancing control is essential to keep the capacitor voltages at the reference value in MMC SMs for upper and lower arm.

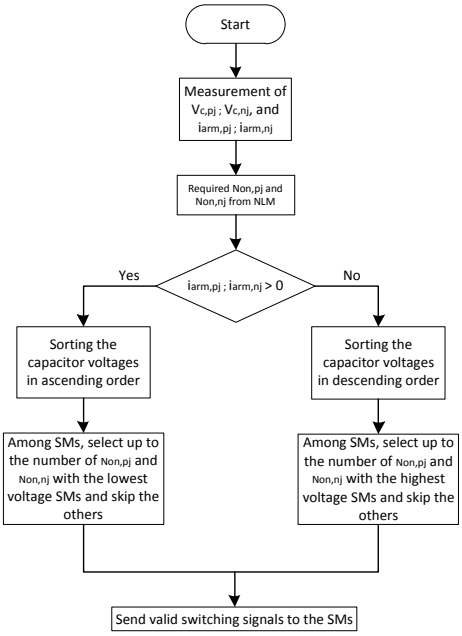

Figure 8. Capacitor voltage balancing algorithm

For this purpose, balancing algorithm should be implemented for the arms. In case of the capacitor voltages are not sufficiently balanced, not only MMC output parameters adversely affected, but also semiconductor devices in MMC can be damaged. Balancing algorithm is shown in Fig. 8. This algorithm is based on the principle of measuring and sorting the SM capacitor voltages and selecting the appropriate SMs. After measuring the capacitor voltages, according to the direction of arm current, they are sorted from highest voltage capacitors to lowest voltage or lowest voltage capacitors to highest voltage. After determining the required number of SMs with the data obtained from NLM, and completing the ascending/descending order process, proper SM capacitors are selected to be charged/discharged. Aforementioned capacitor voltage balancing is practically and successfully carried out using the proposed digital control scheme as illustrated in Fig. 9. SM selection part in the proposed control scheme is also important and it is not the specific topic of this paper. With digital operations performed at each sampling cycle, capacitor voltages are balanced and kept constant.

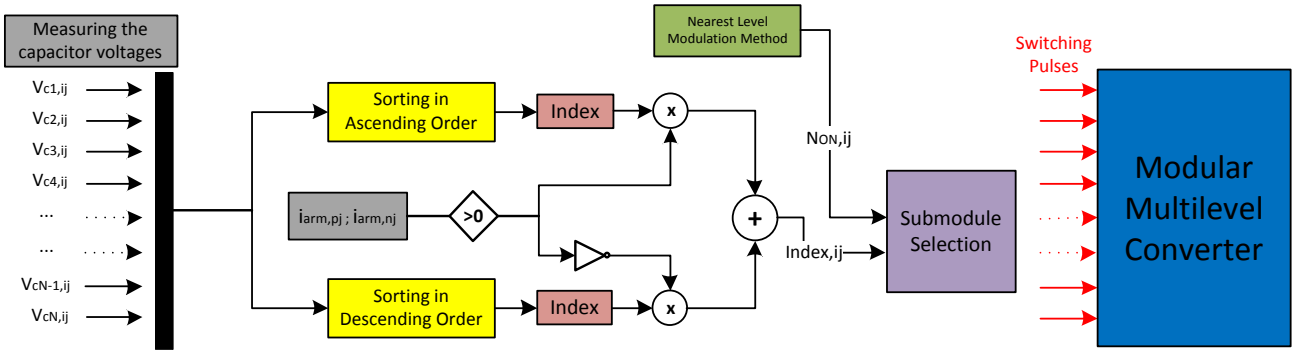

Figure 9. The proposed capacitor voltage balancing scheme under NLM

Different load groups are activated/deactivated in the MMC based WECS that cause the voltage change at the PCC. Hence, voltage at the PCC should be effectively controlled. In addition, frequency of the load voltage should be constant. In this context, both voltage and frequency stabilization should be provided for reliable operation under dynamics variations. For this reason, dq synchronous rotating reference frame-based voltage control scheme using PI controller is presented. Voltage and frequency stabilization at the PCC at the load side is achieved by

regulating the voltage at the reference value. Fig. 10 represents the implemented load voltage control scheme. Transformation in dq frame is a mathematical expression that reduces the three-phase AC quantities of PCC voltage to two DC quantities. With this transformation, time varying signals can be represented as DC signals. After applying abc-dq transformation, dq components of PCC voltage are represented as follows:

$$V_d = \frac{2}{3}\left(V_a \sin(\omega t) + V_b \sin(\omega t - \tfrac{2\pi}{3}) + V_c \sin(\omega t + \tfrac{2\pi}{3})\right) \quad (19a)$$

$$V_q = \frac{2}{3}\left(V_a \cos(\omega t) + V_b \cos(\omega t - \tfrac{2\pi}{3}) + V_c \cos(\omega t + \tfrac{2\pi}{3})\right) \quad (19b)$$

where, V_d and V_q are the components of the dq axis system in the rotating reference frame. After measurement of PCC voltage, the error voltage is computed as:

$$V_{error} = V_{ref} - V_d \quad (20)$$

where, d component is corresponding to the magnitude value of the PCC voltage. In abc-dq transformation, q component of the measured three-phase voltage is nearly zero. Therefore, magnitude of the PCC voltage can be controlled by regulating the d component with PI controller as follows:

$$V_{d\_ref} = K_p(V_{ref} - V_d) + K_i \int (V_{ref} - V_d)dt \quad (21)$$

where, V_{d_ref} is the reference of the modulation process.

IV. Simulation Studies

In this section, in order to confirm the applicability of the presented MMC based WECS topology given in Fig. 4, a simulation model is built. Additionally, the high performance of the suggested control method for the designed model is verified under various case studies.

Main design and controller parameters of the designed system topology are given in Table 2 and Table 3, respectively.

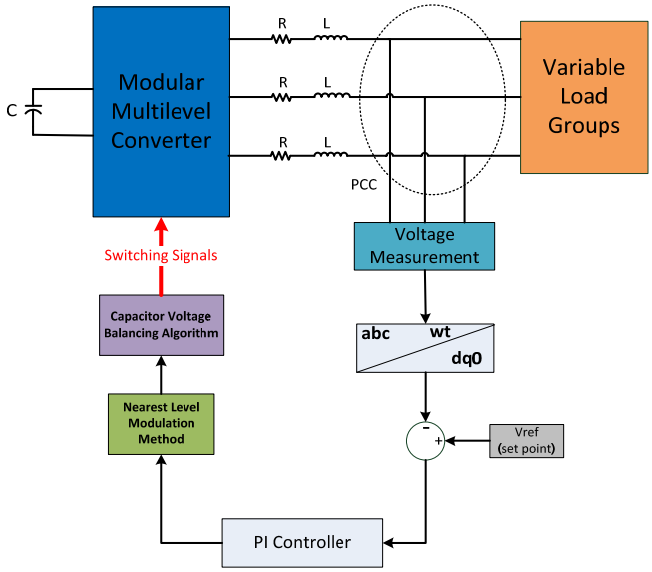

Figure 10. The designed load voltage control scheme

Comprehensive results for the presented study are discussed in case studies given in the subsections below.

A. Case Study 1: Verification of the DC-link Voltage Control Scheme

In this case, performance evaluation of the DC-link voltage control scheme is tested and validated. DC-link voltage is observed while the designed MMC based WECS is running under fixed speed and constant load operation. Only Load 1 is used in this case.

Accordingly, in Fig. 11, the rotational speed of the PMSG is given, which is equal to nearly 78.54 rad/s that corresponds to the 750 rpm resulting 50 Hz output voltage. Under this condition, the designed MMC based WECS topology is run by dynamically changing the reference value of the DC-link. Fig. 12 indicates the good performance of the designed controller. In this regard, reference point is varied with 4 seconds interval as 800 V, 1000 V and 600 V, respectively. The voltage ripple of the DC-link voltage is obtained as nearly 0.25%.

This result also shows the satisfactory performance of the designed DC-link voltage controller. In all dynamic variations, actual DC-link voltage is stable and follows the reference value, and this result demonstrates the effectiveness of the designed DC-link voltage control scheme.

Table 2: Main Design Parameters

Parameter	Value
PMSG	
Rated voltage in line-line	600 V
Number of poles	8
Flux linkage	0.87 Wb
Stator phase resistance	0.0918 Ω
Armature inductance	0.975 mH
Inductance of boost converter	9.2 mH
MMC	
DC-link voltage	800 V
DC-link capacitor	878 uF
System frequency	50 Hz
Number of SMs	4
Arm inductance	5 mH
SM capacitance	10 mF
SM capacitor voltage	200 V
Sampling frequency	100 kHz
Load Side	
R, L, C (Coupling)	0.01 Ω, 20 mH, 100 uF
Load 1	9 Ω + 2.5 mH
Load 2	90 Ω + 3 mH

Table 3: Controller Parameters

Control Unit	Value
DC-link Regulator	Kp= 0.01 Ki= 6.5
Load Voltage Regulator	Kp= 0.001 Ki= 0.5

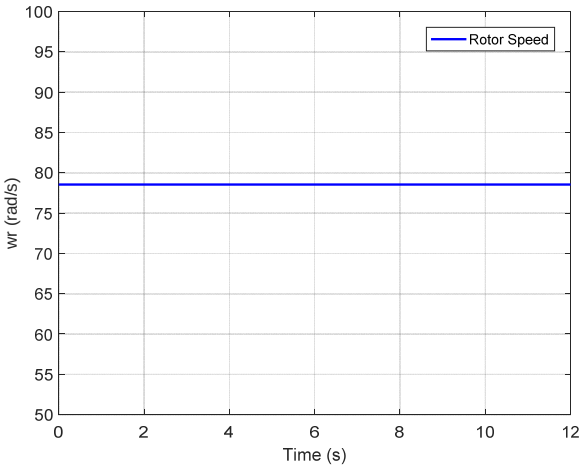

Figure 11. Fixed rotor speed of PMSG

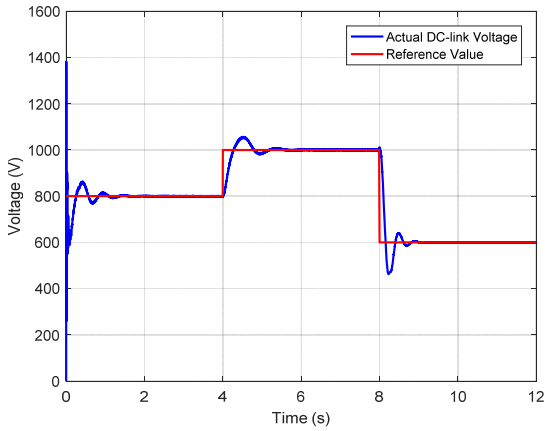

Figure 12. Dynamic performance of the DC-link voltage control scheme

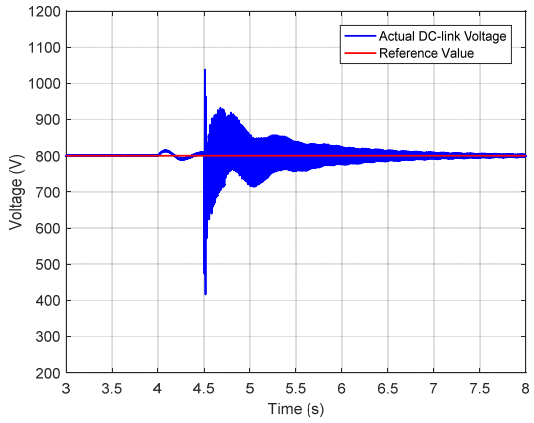

Figure 13. The effect of balancing control scheme on DC-link voltage

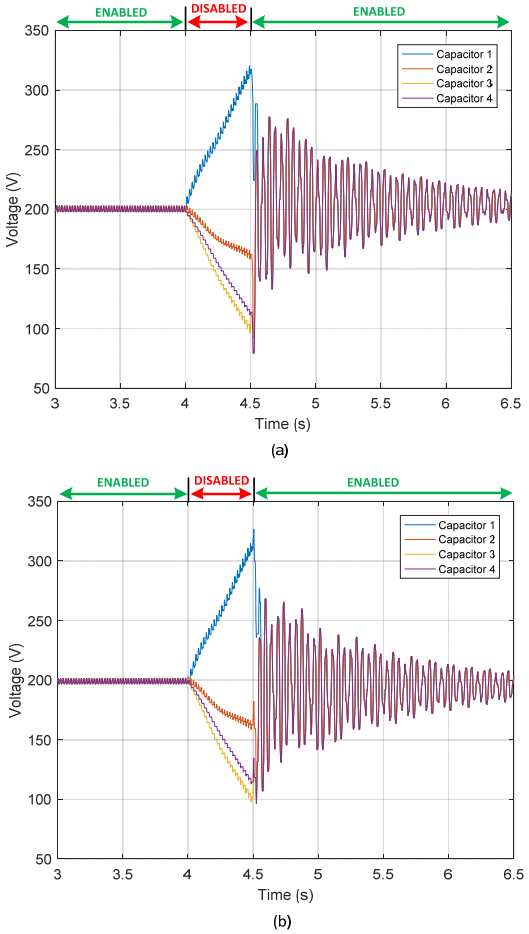

Figure 14. Enabled/disabled mode of capacitor voltage balancing scheme and capacitor voltage waveforms; (a) behavior of upper arm capacitors, (b) behavior of lower arm capacitors

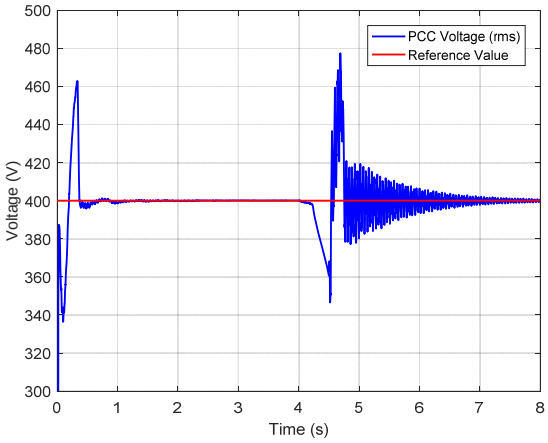

Figure 15. The effect of capacitor voltage balancing scheme on PCC voltage

B. Case Study 2: Verification of the Proposed Capacitor Voltage Balancing Scheme

To show the feasibility of the presented capacitor voltage balancing scheme, a test study is carried out under fixed speed and constant load operation as given in the previous case conditions. Only Load 1 is used in this case. For this reason, the behavior of all capacitor voltages of upper and lower arm for phase-a together with DC-link voltage and PCC voltage at the load side are investigated under the conditions that capacitor voltage balancing scheme is enabled and disabled during the operation of the designed MMC based WECS. The effect of balancing control scheme on system parameters is monitored. This state is indicated by dynamic circumstances in simulation environment. Balancing control scheme is disabled between 4 and 4.5 seconds, then, it is activated again. In Fig. 13, the effect of balancing control scheme on DC-link voltage is observed. DC-link voltage is unstable during the disabled mode while it is re-balanced during the enable mode. As can be deduced from Fig. 14, all capacitor voltages of each arm remain at reference value during the enabled mode. Arm energy is equally shared among the capacitors so that voltage waveforms are almost the same as each other. Otherwise, voltage of capacitor 1 increases while other capacitor voltages decrease, that causes unbalanced operation during the disabled mode.

When the balancing control scheme is activated again, all capacitor voltages are successfully balanced in both arms. Time interval of disabled mode is important to re-balance the capacitor voltages. In this regard, capacitor voltages of arms are gradually approaching to 200 V in about 2 seconds for 0.5 seconds disabled mode. The voltage ripple of the balanced capacitor voltages is approximately obtained as 1.5%. This result also denotes the efficient performance of the presented balancing scheme. Moreover, the impact of the balancing control scheme on PCC voltage at the load side is investigated. In balanced conditions, PCC voltage is set at 400 V through the load voltage control scheme. As given in Fig. 15, PCC voltage continuously decreases until almost 360 V during the disabled mode while it is stabilized during the enabled mode. According to the aforementioned simulation studies, the suitability of the proposed balancing scheme is validated by showing successful capacitor voltage control.

C. Case Study 3: Verification of the Load Voltage Control Scheme

A case study is performed to show the practicality of the presented load voltage control scheme under fixed speed and variable load operation in this subsection. Load 1 and 2 are used in this case. PCC voltage and its frequency are regulated using dq synchronous rotating reference frame-based voltage control scheme with PI controller. For this purpose, to ensure the reference voltage at the PCC, modulation index is generated via the controller. Load 1 is operated in the whole simulation process while load 2 is added and activated in the system at fifth seconds during the simulation. Also, reference value for PCC voltage is changed from 400V to 380V line-to-line at tenth seconds while the system frequency is continuously 50 Hz. Accordingly, in Fig. 16, the modulation index variation is given, which is adaptive to obtain the reference value at the PCC under dynamic load and reference change conditions. The modulation index is initially nearly 0.87. Then, due to the load change, the modulation index is increased to 0.91 while it is nearly 0.86 to obtain 380V under the reference change. PCC voltage and frequency are depicted in Fig. 17 under transient changes. As illustrated, PCC voltage is successfully regulated at 400V and 380V at 50Hz. In this case study, it is shown that PCC voltage is constant and voltage and frequency stabilization at the PCC are accomplished with the voltage control scheme.

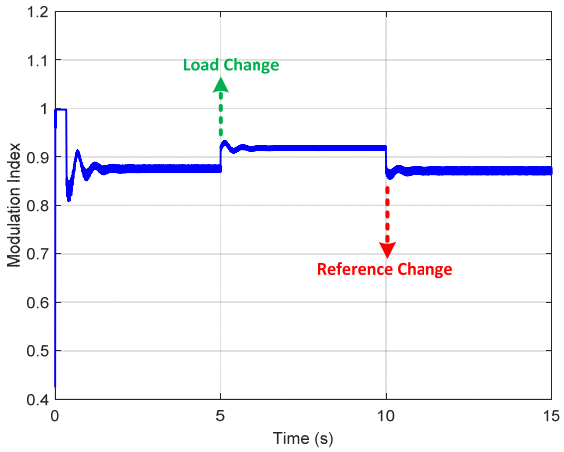

Figure 16. The modulation index generated by the load voltage control feedback system

D. Case Study 4: Overall Performance of the Designed MMC based WECS

In this case study, the designed MMC based WECS is operated and its performance evaluation is presented under variable speed and load change scenarios. PMSG is driven to obtain different wind speed conditions under different rotational speed values by changing the rotor speed of the generator. In this context, as given in Fig. 18, in order to obtain different output voltages having also various frequencies, PMSG is run at 78.54 rad/s, 70.68 rad/s and 86.39 rad/s that corresponds to the 50Hz, 45Hz and 55Hz, respectively. The speeds are dynamically changed in the fourth and tenth seconds in the simulated model. Load 1 is operated in the whole simulation process while load 2 is activated in the system at seventh seconds during the simulation. As illustrated in Fig. 19, the output voltage and frequency generated by PMSG vary with respect to the rotor speed, and the voltage has a sinusoidal waveform having low harmonic.

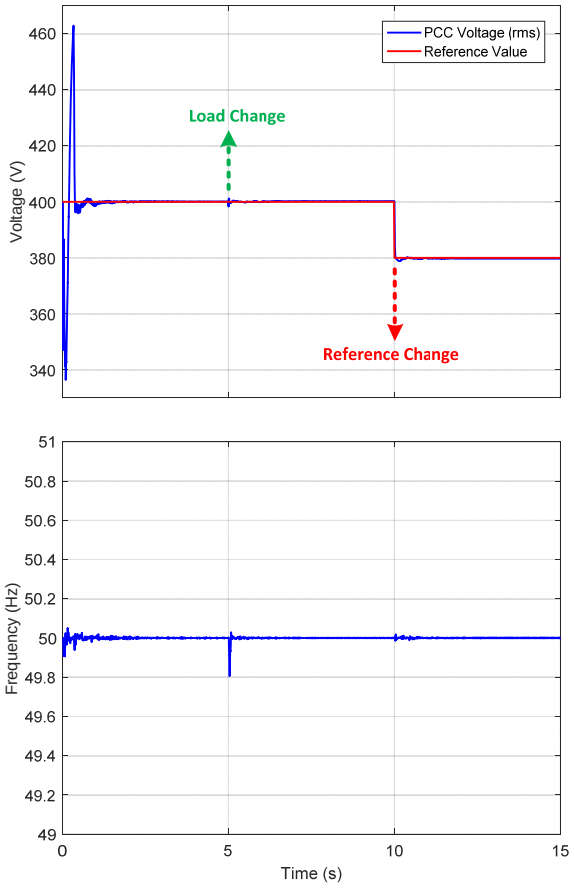

Figure 17. PCC voltage and frequency under load and reference change

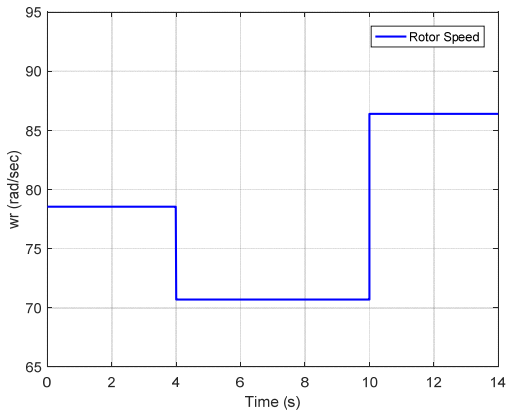

Figure 18. Variable rotor speed of PMSG

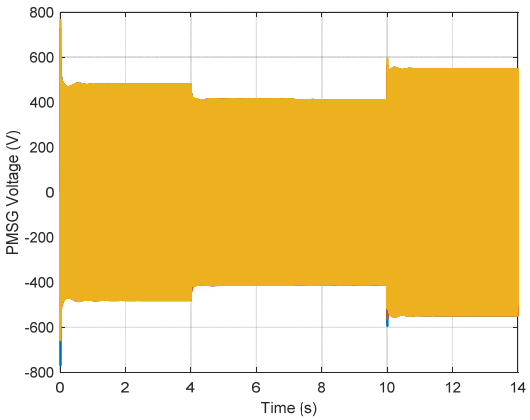

Figure 19. Output voltage of PMSG under different speed regimes

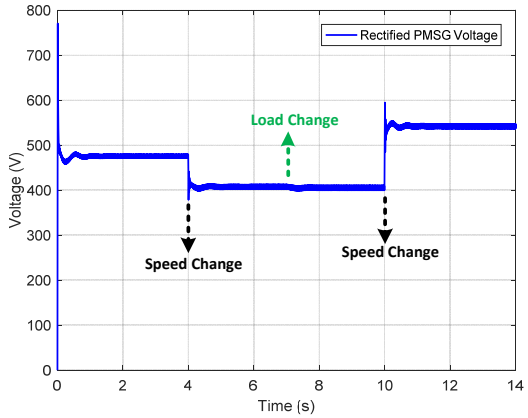

Figure 20. Obtained voltage via diode rectifier

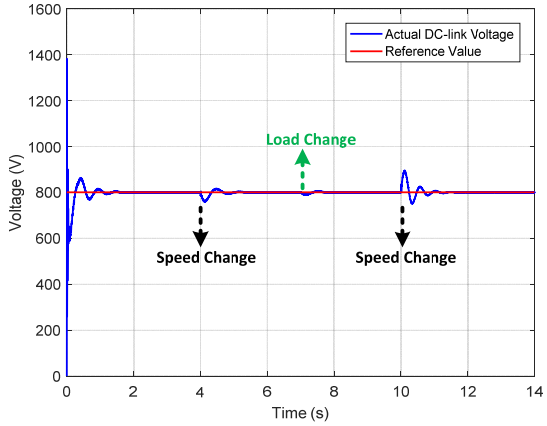

Figure 21. DC-link voltage during the simulation

The frequency is 50Hz, 45Hz and 55Hz in the simulation process. In the first instance, the PMSG voltage is converted to the DC voltage by means of rectifier as captured in Fig. 20. In the second stage, variable DC voltage is increased and controlled by the DC-DC converter. In all dynamic factors such as speed and load change, the actual DC-link voltage is regulated at the reference point. Simulation result of the DC-link voltage is depicted in Fig. 21. The designed controller reacts quickly to follow the set point (800V) under dynamic circumstances. This performance shows that the controller provides a rapid response to the active changes. MMC supplied from DC-link transforms the DC energy into the AC energy for utility and load demands. However, in this vision, arm energy balancing of MMC should be provided by capacitor voltage balancing scheme. Unless arm energy balancing is not achieved, not only the output performance of MMC is adversely affected, but also the semiconductor switching devices in the SMs may be damaged. As mentioned in the previous case study, balancing scheme is implemented in the presented MMC based WECS. The behavior of all capacitor voltages of upper and lower arm for phase-a are presented in Fig. 22(a) and 22(b), respectively. Arm energy is evenly distributed among the capacitors so that voltage waveforms are nearly the same as explained in the section of the verification of the balancing scheme. All of the capacitor voltages are balanced at 200V although there are some transient changes. PCC voltage under dynamic changes is controlled with the help of dq synchronous rotating reference frame-based voltage control scheme with PI controller. The desired PCC voltage as

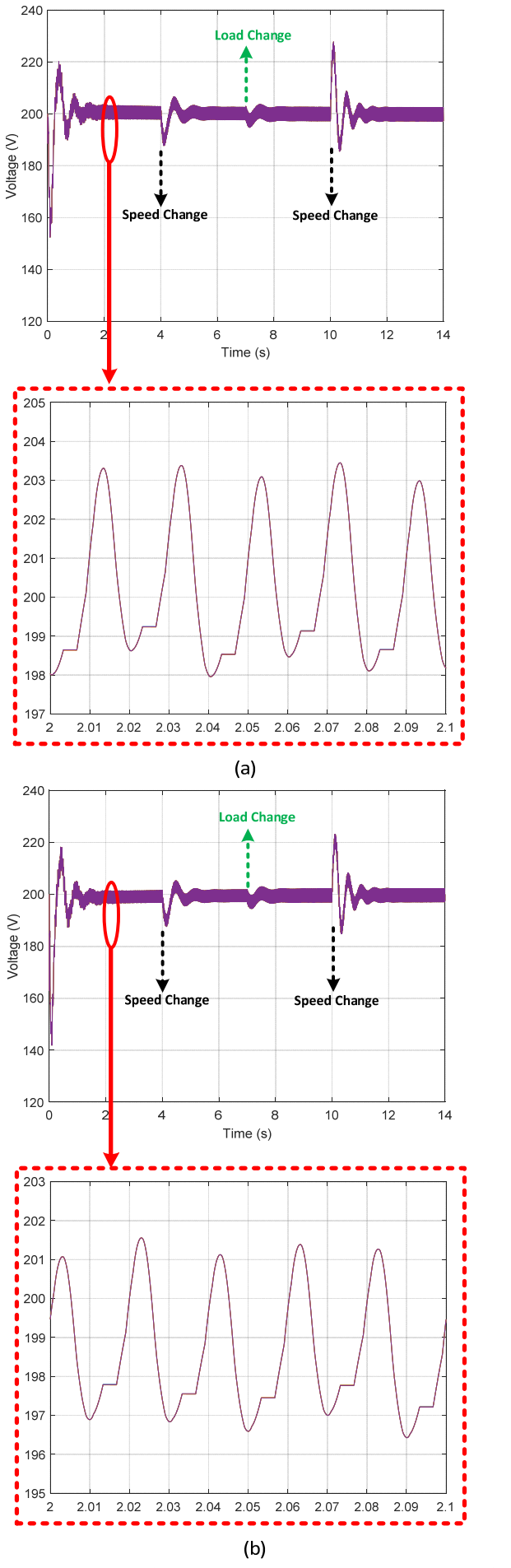

Figure 22. Capacitor voltage waveforms; (a) upper arm capacitors, (b) lower arm capacitors

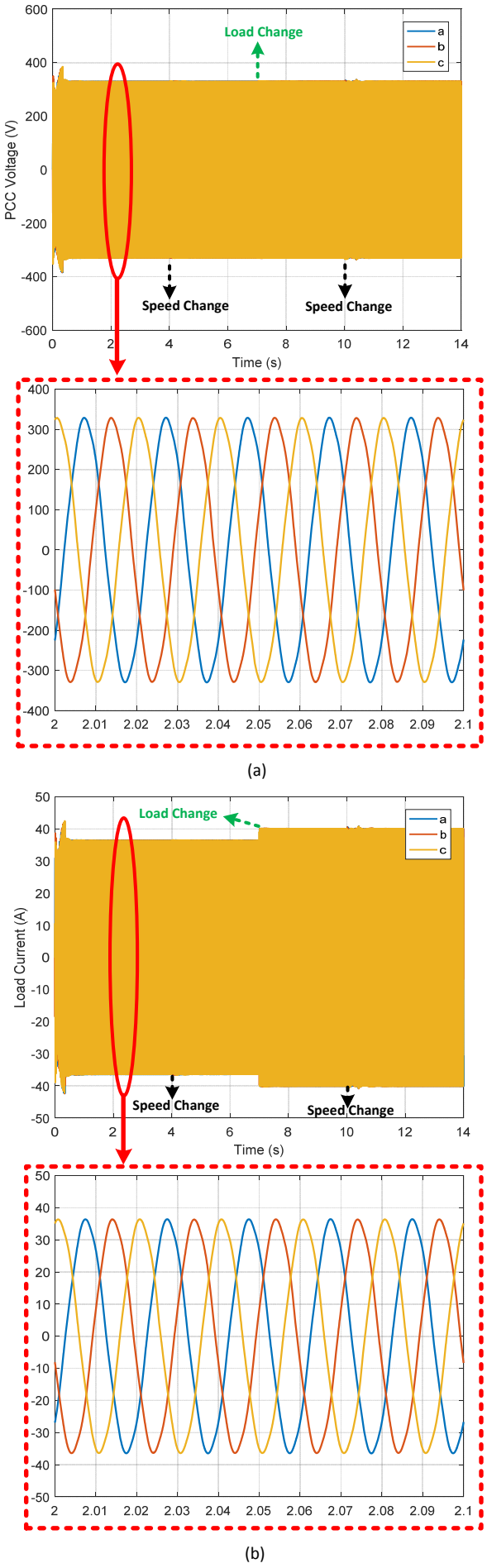

Figure 23. PCC voltage and load current waveforms; (a) PCC voltage, (b) load current

400V line-to-line at 50Hz at the PCC is achieved through the designed controller. PCC voltage and load current waveforms are shown in Fig. 23(a) and Fig. 23(b), respectively. From the obtained results, it is shown that PCC voltage is kept constant and voltage and frequency stabilization at the PCC are accomplished.

V. Experimental Study

In order to validate the effectiveness of the proposed capacitor voltage balancing scheme under NLM, a prototype of a single-phase MMC circuit topology consisting of four SMs per arm is built as seen in Fig. 24. Table 4 presents the circuit parameters used for the experiment. In the experimental prototype, main DC source is employed at the DC side to feed the MMC topology and power unit supplies the experiment boards. Herein, the PMSG and DC-DC boost converter part is not used and emulated using the constant DC source. In this way, a constant DC voltage is applied to the MMC topology. Atmel microcontroller board and Xilinx FPGA circuit development platform are utilized to control the MMC topology. MMC SMs contain isolated gate driver circuits, MOSFET power switches and capacitors. Measurement cards include the voltage and current sensors, which measures the capacitor voltages of each SM and arm current of the upper and lower arm. Then, microcontroller analog ports receive these data and process them in the embedded balancing method. Thereafter, microcontroller delivers the necessary digital information to the FPGA using serial line for switching of the MOSFETs. In this way, FPGA controller generates the triggering signals for the each SM of MMC. Sampling cycle of FPGA controller is selected as 1 kHz. A dead time of 200 ns is used for switching of MOSFETs. The output voltage and current waveform are monitored by using digital oscilloscope. Additionally, constant resistive-inductive load whose values are given in Table 4 is established to emulate the constant load of operation.

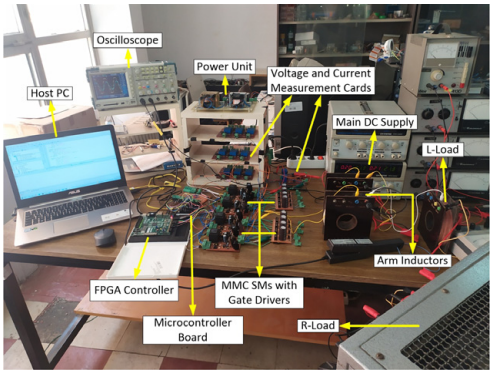

Figure 24. Experimental setup of the MMC topology

TABLE 4: Experimental Circuit Parameters of the MMC System

Parameter	Value
DC-link voltage	40 V
Output frequency	50 Hz
Number of SMs	4
Arm inductance	29 mH
SM capacitance	4.7 mF
Voltage sensor, LEM LV 25-P	Up to 500 V
Current sensor, LEM LA 55-P	Up to 50 A
Load resistance	10 Ω
Load inductance	15 mH

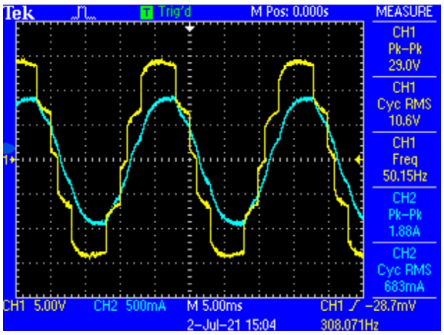

Figure 25. Output voltage and current waveform

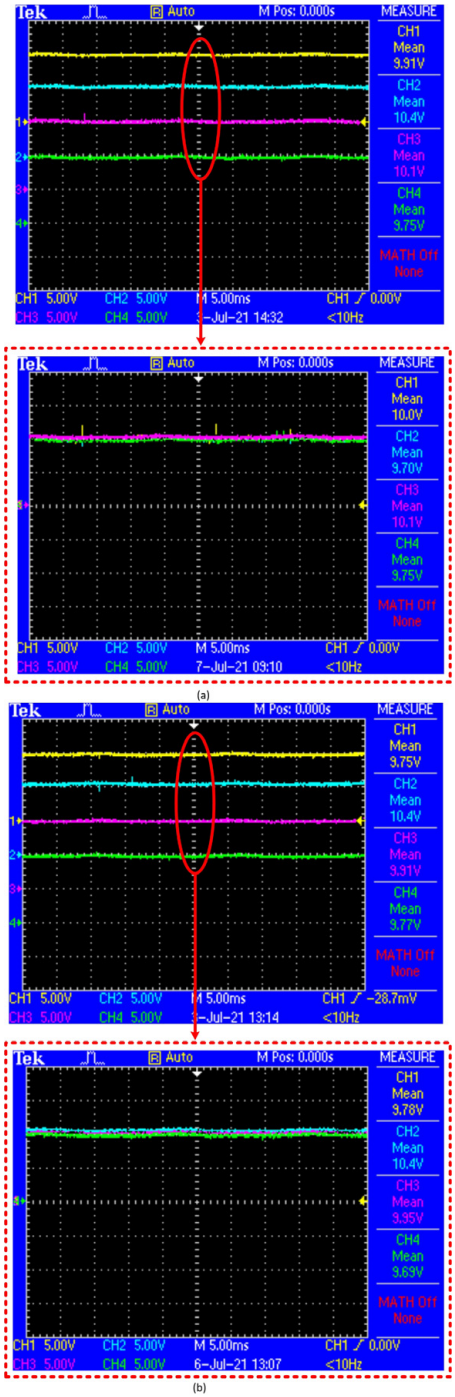

Figure 26. Balanced capacitor voltages in the experiment; (a) upper arm capacitors, (b) lower arm capacitors

First of all, the output voltage (channel 1) and current (channel 2) waveforms are given in Fig. 25 when the modulation ratio is 1. Also, balanced capacitor voltages of upper and lower arm are presented in Fig. 26(a) and 26(b), respectively. In both figures, capacitor voltages are visualized by different and the same horizontal positions. In the screenshot, all four channels from 1 to 4 correspond to the capacitors from 1 to 4, respectively for the upper and lower arm. Average values of the capacitor voltages on the MMC SMs are kept around 10 V. After all, the proposed capacitor voltage balancing scheme is supported and verified by the experimental results and applicability of it is demonstrated in this section.

VI. Conclusion

In this paper, an efficient capacitor voltage balancing scheme under NLM has been developed for MMC based WECS. Arm energy balancing inside the converter and satisfactory output performance at the PCC are provided through the proposed control scheme. Moreover, DC-link voltage control has been achieved via the designed hysteresis current control based PI controller. Additionally, load voltage control has been accomplished using dq reference frame based voltage control scheme for voltage and frequency stabilization at the PCC. Finally, simulation and experimental results have been provided to confirm the suitability of the developed control scheme under variable dynamic conditions for MMC based WECS.

References

[1] S. D. Ahmed, et al., "Grid integration challenges of wind energy: A review," IEEE Access, vol. 8, pp. 10857-10878, 2020. doi:10.1109/ACCESS.2020.2964896

[2] P. Sadorsky, "Wind energy for sustainable development: Driving factors and future outlook," J. Clean. Prod., vol. 289, pp. 1–15, 2021. doi:10.1016/j.jclepro.2020.125779

[3] M. Cheng, Y. Zhu, "The state of the art of wind energy conversion systems and technologies: A review," Energy Convers. Manag., vol. 88, pp. 332–347, 2014. doi:10.1016/j.enconman.2014.08.037

[4] V. Yaramasu, et al., "High-power wind energy conversion systems: State-of-the-art and emerging technologies," Proceedings of the IEEE, vol. 103, no. 5, pp. 740–788, 2015. doi:10.1109/JPROC.2014.2378692

[5] M. Nasiri, J. Milimonfared, S. H. Fathi, "A review of low-voltage ride-through enhancement methods for permanent magnet synchronous generator based wind turbines," Renew. Sustain. Energy Rev., vol. 47, pp. 399–415, 2015. doi:10.1016/j.rser.2015.03.079

[6] L. Pan, C. Shao, "Wind energy conversion systems analysis of PMSG on offshore wind turbine using improved SMC and extended state observer," Renew. Energy, vol. 161, pp. 149–161, 2020. doi:10.1016/j.renene.2020.06.057

[7] W. Du, W. Dong, H. F. Wang, "Small-signal stability limit of a grid-connected PMSG wind farm dominated by the dynamics of PLLs," IEEE Trans. Power Syst., vol. 35, no. 3, pp. 2093–2107, 2020. doi:10.1109/TPWRS.2019.2946647

[8] S. Grabic, N. Celanovic, V. A. Katic, "Permanent magnet synchronous generator cascade for wind turbine application," IEEE Trans. Power Electron., vol. 23, no. 3, pp. 1136–1142, 2008. doi:10.1109/TPEL.2008.921181

[9] N. Herisanu, et al., "Dynamic response of a permanent magnet synchronous generator to a wind gust," Energies, vol. 12, no. 5, pp. 1–11, 2019. doi:10.3390/en12050915

[10] F. Blaabjerg, K. Ma, "Future on power electronics for wind turbine systems," IEEE J. Emerg. Sel. Top. Power Electron., vol. 1, no. 3, pp. 139–152, 2013. doi:10.1109/JESTPE.2013.2275978

[11] S. Kouro, et al., "Recent advances and industrial applications of multilevel converters," IEEE Trans. Ind. Electron., vol. 57, no. 8, pp. 2553–2580, 2010. doi:10.1109/TIE.2010.2049719

[12] J. Rodríguez, et al., "Multilevel voltage-source-converter topologies for industrial medium-voltage drives," IEEE Trans. Ind. Electron., vol. 54, no. 6, pp. 2930–2945, 2007. doi:10.1109/TIE.2007.907044

[13] M. Kurtoğlu, et al., "Recent contributions and future prospects of the modular multilevel converters: A comprehensive review," Int. Trans. Electr. Energy Syst., vol. 29, 2019. doi:10.1002/etep.2763

[14] N. Güler, et al., "An inverter design for a new permanent magnet synchronous generator," Int. J. Hydrogen Energy, vol. 42, no. 28, pp. 17723–17732, 2017. doi:10.1016/j.ijhydene.2017.01.223

[15] R. Bharanikumar, A. N. Kumar, "Performance analysis of wind turbine-driven permanent magnet generator with matrix converter," Turkish J. Electr. Eng. Comput. Sci., vol. 20, no. 3, pp. 299–317, 2012. doi:10.3906/elk-1008-684

[16] M. Diaz, et al., "Control of wind energy conversion systems based on the modular multilevel matrix converter," IEEE Trans. Ind. Electron., vol. 64, no. 11, pp. 8799–8810, 2017. doi:10.1109/TIE.2017.2733467

[17] S. Debnath, M. Saeedifard, "A new hybrid modular multilevel converter for grid connection of large wind turbines," IEEE Trans. Sustain. Energy, vol. 4, no. 4, pp. 1051–1064, 2013. doi:10.1109/TSTE.2013.2266280

[18] R. K. Swami, P. Samuel, R. Gupta, "Power control in grid-connected wind energy system using diode-clamped multilevel inverter," IETE J. Res., vol. 62, no. 4, pp. 515–524, 2016. doi:10.1080/03772063.2015.1083908

[19] L. Fateh, et al., "Modeling and control of a permanent magnet synchronous generator dedicated to standalone wind energy conversion system," Front. Energy, vol. 10, no. 2, pp. 155–163, 2016. doi:10.1007/s11708-016-0410-1

[20] C. N. Bhende, S. Mishra, S. G. Malla, "Permanent magnet synchronous generator-based standalone wind energy supply system," IEEE Trans. Sustain. Energy, vol. 2, no. 4, pp. 361–373, 2011. doi:10.1109/TSTE.2011.2159253

[21] Y. Wang, et al., "Application of modular multilevel converter in medium voltage high power permanent magnet synchronous generator wind energy conversion systems," IET Renew. Power Gener., vol. 10, no. 6, pp. 824–833, Jul. 2016. doi:10.1049/iet-rpg.2015.0444

[22] X. Xie, et al., "Analysis of power loss and reliability on hybrid modular multilevel converter with redundancy configuration for offshore wind turbines," 2019 International Conference on Electrical Machines and Systems (ICEMS), pp. 1–6, 2019. doi:10.1109/ICEMS.2019.8921465

[23] F. B. Xu, et al., "Modular multilevel converter-based PWM rectifier system for high speed or high frequency permanent magnet synchronous generators," 2018 21st International Conference on Electrical Machines and Systems (ICEMS), Jeju, Korea (South), 2018, pp. 1229–1234. doi:10.23919/ICEMS.2018.8548959

[24] Z. Liu, et al., "Minimal capacitor voltage ripple control for the modular multilevel converter based wind energy conversion system," 2020 15th IEEE Conference on Industrial Electronics and Applications (ICIEA), Kristiansand, Norway, 2020, pp. 1864-1869. doi:10.1109/ICIEA48937.2020.9248295

[25] H. Li, et al., "Cost and reliability optimization of modular multilevel converter with hybrid submodule for offshore DC wind turbine," Int. J. Electr. Power Energy Syst., vol. 120, 2020. doi:10.1016/j.ijepes.2020.105994

[26] A. Kamal, A. Basit, "High power medium voltage PMSG based WECS using three-level boost and modular multilevel converters," 2018 International Conference on Power Generation Systems and Renewable Energy Technologies (PGSRET), Islamabad, Pakistan, 2018, pp. 1-6. doi:10.1109/PGSRET.2018.8685943

[27] Z. Liu, et al., "A steady-state analysis method for modular multilevel converters connected to permanent magnet synchronous generator-based wind energy conversion systems," Energies, vol. 11, no. 2, pp. 1–31, 2018. doi:10.3390/en11020461

[28] M. M. N. Amin, O. A. Mohammed, "DC-Bus Voltage Control Technique for Parallel-Integrated Permanent Magnet Wind Generation Systems," IEEE Trans. Energy Convers., vol. 26, no. 4, pp. 1140-1150, 2011. doi:10.1109/TEC.2011.2163409

[29] S. G. Malla, C. N. Bhende, "Voltage control of stand-alone wind and solar energy system," Int. J. Electr. Power Energy Syst., vol. 56, pp. 361-373, 2014. doi:10.1016/j.ijepes.2013.11.030

[30] A. E. Leon, S. J. Amodeo, "Energy balancing improvement of modular multilevel converters under unbalanced grid conditions," IEEE Trans. Power Electron., vol. 32, no. 8, pp. 6628–6637, Aug. 2017. doi:10.1109/TPEL.2016.2621000

[31] A. Dekka, et al., "Integrated model predictive control with reduced switching frequency for modular multilevel converters," IET Electr. Power Appl., vol. 11, no. 5, pp. 857–863, 2017. doi:10.1049/iet-epa.2016.0454

[32] S. Ghasemi, A. Tabesh, J. Askari-Marnani, "Application of fractional calculus theory to robust controller design for wind turbine generators," IEEE Trans. Energy Convers., vol. 29, no. 3, pp. 780–787, 2014. doi:10.1109/TEC.2014.2321792

[33] K. Suresh, D. R. Arulmozhiyal, "Design and implementation of bi-directional DC-DC converter for wind energy system," Circuits Syst., vol. 7, no. 11, pp. 3705–3722, 2016. doi:10.4236/cs.2016.711311

[34] A. Chatterjee, K. B. Mohanty, "Current control strategies for single phase grid integrated inverters for photovoltaic applications-a review," Renew. Sustain. Energy Rev., vol. 92, pp. 554–569, 2018. doi:10.1016/j.rser.2018.04.115

[35] G. Konstantinou, et al., "Switching frequency analysis of staircase-modulated modular multilevel converters and equivalent PWM techniques," IEEE Trans. Power Deliv., vol. 31, no. 1, pp. 28–36, Feb. 2016. doi:10.1109/TPWRD.2015.2416759

[36] S. Du, A. Dekka, B. Wu, N. Zargari, Modular Multilevel Converters: Analysis, Control, and Applications. John Wiley & Sons, 2017